X-ray Photoelectron Spectroscopy in the Study of Polyelectrolyte Adsorption on Mica and Cellulose

Orlando J. Rojas,*,† Marie Ernstsson,‡ Ronald D. Neuman,§ and Per M. Claesson‡,||

Escuela de Ingeniería Química, Lab. FIRP, Universidad de Los Andes, Mérida 5101, Venezuela, Institute for Surface Chemistry, Box 5607, SE-114 86 Stockholm, Sweden, Chemical Engineering Department, Auburn University, Auburn, Alabama 36849, and Department of Chemistry, Surface Chemistry, Royal Institute of Technology, SE-100 44 Stockholm, Sweden

Received: May 8, 2000

X-ray photoelectron spectroscopy was used to estimate the absolute amount of cationic polyelectrolytes that adsorbs on mica and cellulose surfaces in aqueous media. The calculation takes advantage of the knowledge of the mica crystal composition at the basal plane and its ion-exchange properties in aqueous solution. The XPS was operated under monochromatic and unmonochromatic mode and good agreement was observed in the resulting adsorbed amount. The evaluation of the amount of cationic polyelectrolyte adsorbed on cellulose was achieved using calibration curves obtained from adsorption data for the same polyelectrolytes on bare mica surfaces. The adsorption isotherm for polyelectrolytes of low charge density adsorbed on cellulose reveals that their affinity toward cellulose is weaker compared to that observed for highly charged surfaces such as mica. The effect of the polyelectrolyte charge density on the adsorbed amount and the number density of charged segments adsorbed on cellulose were also investigated. From these results it can be concluded that nonelectrostatic interactions are the main contributors to the adsorption of polyelectrolytes on cellulose, but it cannot be ruled out that electrostatic effects also take part in the adsorption mechanism. Finally, it is demonstrated that it is not correct to use the adsorbed amount of polyelectrolytes to determine the surface charge on cellulose surfaces.

Introduction

Many methods have been devised to characterize polymeric materials in terms of surface composition, spatial organization of the atoms and molecules, surface topography, and mobility of atoms in the surface region. One of the most valuable ones, due to the amount of information it generates, is X-ray photoelectron spectroscopy (XPS).

Many features make XPS desirable as an aid to study polymeric materials. These include the fact that it is essentially nondestructive, provides useful chemical-state and surface information, and allows the use of samples of almost any shape and size. Furthermore, the interpretation of spectra is relatively straightforward. Quantification with XPS is reported to be better than 10% using calibration standards, and has very good reproducibility.[1,2]

XPS has been extensively used in studies involving cellulose-related surfaces. Most of the reported investigations deal with paper coating,[3] sizing [4−8] and general cellulosic substrates.[9−13] Its application to study cellulosic substrates has steadily increased since the first reported investigations on the subject by Dorris and Gray.[9−11] Related studies have involved the surface composition and surface chemistry of fibers[10,14,15] and adsorption of polymers,[16] and other additives (e.g., stearic acid).[17]

The use of XPS to study polymer adsorption on surfaces is obviously amply justified. When used in the standard way this technique is, however, limited to the quantification on a relative basis, of the adsorbed amount. It is therefore highly desirable to develop a methodology that allows absolute quantification at the same time as chemical and compositional information is obtained. In this way the XPS potential would be further expanded to access the problem of polymer adsorption at solid/liquid interfaces.

In this investigation we illustrate how quantitative information on the adsorbed amount of polyelectrolytes on mica can be obtained from XPS measurements. Finally, the results obtained for mica surfaces are used as a calibration standard for evaluation of the adsorption of polyelectrolytes on cellulose. In particular, the effect of the polyelectrolyte charge density on their adsorption on Langmuir−Blodgett cellulose films is quantified.

Experimental Section

Materials and Methods. The polyelectrolytes used in this investigation were random copolymers of uncharged acrylamide (AM) and positively charged [3-(2-methylpropionamido)propyl] trimethylammonium chloride (MAPTAC) (see Figure 1). By balancing the ratio MAPTAC/AM in the (radical) copolymerization process, macromolecules with different charge densities (percentage molar ratio of cationic monomers) were synthesized and kindly provided by the Laboratoire de Physico-Chimie Macromoleculaire (Paris). In Table 1, a list of the studied polyelectrolytes along with their charge densities (or cationicity, τ) and molecular weight is provided. For convenience, the polyelectrolytes are referred to as "AM-MAPTAC-X" where X is a number which indicates the respective percentage charge density (e.g., AM-MAPTAC-100 is poly(MAPTAC), with no AM units). Note that in this study both low- and high-charge-density polyelectrolytes were considered.

* Corresponding author. Fax: +58-74-402957. E-mail: rojasoj@ula.ve.
† Universidad de Los Andes.
‡ Institute for Surface Chemistry.
§ Auburn University.
|| Royal Institute of Technology.

10.1021/jp001674z CCC: $19.00
Published on Web 10/10/2000

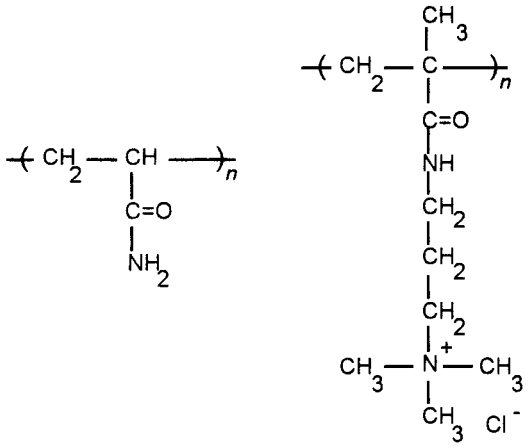

Figure 1. Molecular structure of the monomer AM (left) and MAPTAC (right).

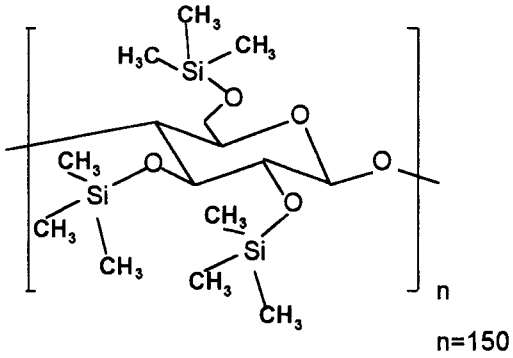

Figure 2. Monomeric unit of the trimethylsilyl cellulose (TMSC).

For preparation of cellulose surfaces a stock solution of 4 mg of trimethylsilyl cellulose (TMSC, see Figure 2) in 10 mL of hexane (Merck, p.a.) was prepared. The TMSC was kindly provided by Prof. Wegner's group (Max-Planck-Institut für Polymerforschung, Mainz) who synthesized it by silylation of microcrystalline cellulose with hexamethyl disilazane.[18]

The deposition of TMSC on the substrate (mica) requires the hydrophobization of the surface, which was accomplished by deposition of a 1:1 mixture of arachidic acid (AA) (Merck) and eicosylamine (EA) (synthesized as described by Berg et al.[19]) using the Langmuir−Blodgett (LB) technique. Equal amounts of AA and EA were dissolved in chloroform (Merck, p.a. grade), containing 5% ethanol, to obtain a 1.35 mM stock solution which was used during LB depositions (to be described later).

Potassium bromide (pro-analysis grade) from Merck was roasted for 24 h at 500 °C before use to remove organic contaminants. Water used in all the experiments was first purified by a reverse osmosis unit (Milli-RO 10 Plus), which includes depth filtration, carbon adsorption, and decalcination. A Milli-Q Plus 185 unit was then used to treat the water with UV light and with a Q-PAK unit consisting of an activated carbon column, a mixed-bed ion exchanger, and an Organex cartridge with a final 0.22-μm Millipack 40 filter.

Prior to use, all glassware was left overnight in chromosulfuric acid followed by extensive rinsing with Milli-Q water. TEFZEL test tubes used in the adsorption/desorption experiments were

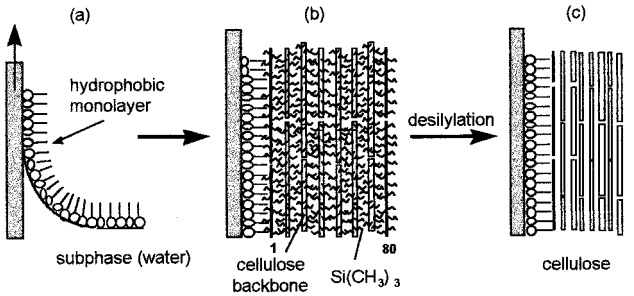

Figure 3. Schematics of the preparation of cellulose substrates: mica hydrophobation by Langmuir−Blodgett (LB) deposition of AA/EA (a); deposition of 80 layers of TMSC (b), and final desilylation (c).

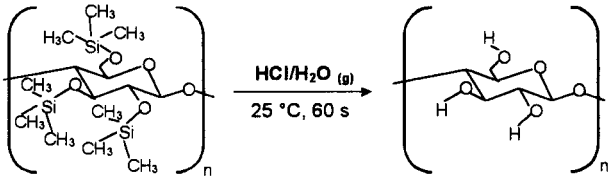

Figure 4. Desilylation of TMSC in humic hydrochloric acid.

cleaned with a SDS micellar solution followed by repeated ethanol and water washings.

Substrate Preparations. Muscovite mica from Reliance Co. (NY) was used as substrate in all the experiments. Pieces of the mica were cleaved several times on both sides in a laminar flow cabinet until an adequate thickness was obtained. All the tools employed were previously cleaned, and protective clothing and gloves were worn to minimize contamination on the high-energy mica surfaces.

The cellulose surfaces were prepared by first depositing TMSC on mica using an automated Langmuir−Blodgett balance (KSV Instruments, Finland) according to procedures by Holmberg et al.[20] In brief, an insoluble monolayer of a 1:1 mixture of AA/EA in chloroform was first spread on a water subphase and transferred onto the mica pieces in an upstroke mode at a constant speed and at a constant surface pressure of 30 mN/m (which yields a surface density of 0.2 nm^2 per hydrocarbon chain) (see Figure 3a). After cleaning the trough and replacing the subphase, eighty layers of TMSC were subsequently LB-deposited at a constant surface pressure of 15 mN/m (which corresponds to a 0.60−0.65 nm^2 area per monomer unit) on the previously hydrophobized mica pieces (see Figure 3b). In all cases, and prior to any monolayer spreading, a reduction in surface pressure lower than 0.1 mN/m (upon surface compression with a Delrin barrier) was used as a check for subphase (water) purity.

TMSC was then converted to cellulose by cleavage of Si−O bonds (Figure 3c) by desilylation for 1 min in the vapor phase above a 10% aqueous HCl solution.[21] The byproduct, trimethylsilyl chloride, is immediately hydrolyzed to trimethylsilanol. In acid media, trimethylsilanol condenses into hexamethyldisiloxane which due to its volatility is released through the film and therefore TMSC is converted to cellulose throughout the layers (see Figure 4).

Adsorption Experiments. In typical experiments with XPS, aqueous solutions of the polyelectrolyte at different concentra-

TABLE 1: Charge Density (τ) and Molecular Weight of the Investigated Polyelectrolytes

polyelectrolyte	τ (theoretical), %	τ (elemental analysis), %	τ (potentiometry), %	τ (NMR), %	MW
AM-MAPTAC-1	1	0.5	0.98		900 000
AM-MAPTAC-10	10	10	9	8.9−9.5	1 000 000
AM-MAPTAC-30	30	31	31	24.2−25.6	780 000
AM-MAPTAC-100	100	99	95		480 000

tions (5−500 μg/mL) were prepared by dilution of a ca. 2000 μg/mL polyelectrolyte stock solution (with 0.1 mM KBr background electrolyte). The substrate (freshly cleaved mica or cellulose deposited on mica) of 5 × 1 cm size, was immersed in the respective polyelectrolyte solution contained in TEFZEL test tubes for an equilibration time of 18−24 h. Finally, the excess solution was eliminated by a nitrogen jet. The size of the sample was reduced to about 2 × 1 cm for XPS analysis.

X-ray Spectrometer. The X-ray photoelectron spectrometer (Kratos Analytical, AXIS-HS) used in this investigation consisted of an Al Kα X-ray (1486.6 eV) source with a hemispherical analyzer. Two modes of operation, referred to as Al-*elstat* and Al-*mono*, were employed. In Al-*elstat* unmonochromatized Al Kα X-rays are created from a dual anode. In this case, the irradiated area is relatively large (in the order of several cm^2) and the electrostatic lens is used to collect the photoelectrons (the analyzed area is also relatively large, in the order of 1 cm^2). Due to the large analyzed area and the close proximity between the sample and the dual anode, the signal intensities (or raw areas) in this operational mode are relatively large.

In Al-*mono* the irradiated X-rays pass through a monochromator which selects an individual X-ray line from the unresolved Kα1,2 doublets, and reduces the spectral background (due to the elimination of X-ray satellite peaks and removal of the Bremsstrahlung). This mode of operation utilizes the dispersion of X-ray energies by diffraction in a crystal according to the well-known Bragg equation:

$$n\lambda = 2d \sin\theta \tag{1}$$

where n is the diffraction order; λ, the X-ray wavelength; d, the crystal spacing; and θ, the Bragg angle.

The monochromatic X-rays then irradiate a small area of the sample (of the order of a few square mm). The analyzed area, using the so-called slotM (magnetic) lens, is under 1 mm^2. In this operational mode the widths of the peaks are reduced and therefore high-resolution spectra (in the order of 1.5 eV) can be achieved.

Because only a small portion of the total X-ray emission is selected in a monochromator and since the distance between the anode and the sample is much larger than in the case of the Al-*elstat* mode, the photon flux on the sample is much less than that from a conventional unmonochromatized source for the same power dissipation.

In all samples, survey scans for peak identification and detail scans for C 1*s*, K 2*s*, K 2*p*, Si 2*p*, and N 1*s* were obtained (in a few cases, detailed scans for Na 1*s* were also obtained). The photoelectron takeoff angle, i.e., the angle between the sample plane and the analyzer, was 90°. However, some samples were run at 30° and 45° as well in order to check the angular dependence of the intensities of the peaks. When operating in Al-*mono* mode the inherent weak signals were subjected to multiple scans to improve the signal-to-noise ratio.

Quantification of the Adsorbed Amount by XPS. XPS techniques have been used for different purposes in surface science. Of our concern is the estimation of the polyelectrolyte adsorbed amount on solid substrates. The surface concentration of different components, however, has been commonly calculated by XPS on a relative basis, often reported as atomic percent, implicitly making the erroneous assumption that all elements from the substrate and overlayer have an equal distribution in the surface region. In this section a procedure is described that can be used to quantify the adsorbed amount on an absolute basis by taking advantage of known surface properties of mica minerals.

The quantification of an element A in a given sample by means of XPS is achieved by measuring the intensity of photoelectrons I_A, of kinetic energy E_A excited by X-rays according to eq 2:[22,23]

$$I_A = D(E_A)\cdot L_A \cdot T(E_A)\cdot Y_A \cdot G(J_A)\cdot A_A \cdot \sigma_A(h\nu) \times \int_0^{x_0} n_A(x)\exp\left(-\frac{x}{\lambda_M(\sin\theta)}\right)dx \tag{2}$$

where D is the detection efficiency for each electron transmitted by the spectrometer; L_A is the angular asymmetry of the photoemission intensity (a spectrometer and atomic parameter); T is the analyzer transmission (an instrumental parameter); Y is the efficiency in the photoelectron process resulting in photoelectrons with the expected energy (an atomic constant); $G(J_A)$ is a function of the X-ray line flux J, over the analyzed area, A (an instrumental parameter); $\sigma_A(h\nu)$ is the atomic cross section; $n_A(x)$ is the number density of atoms A ($n_A = N_A$/matrix volume) which is assumed to depend only on the distance from the surface, x; λ_M is the inelastic mean free path in the sample matrix M; E_A the emitted photoelectrons kinetic energy, and θ is the photoelectron takeoff angle. D, G, A, and Y depend on the spectrometer setup and are not normally known, but they vary little during a measurement.

This led Wagner[24] to propose the use of experimental atomic sensitivity factors S for quantitative XPS analysis. In principle the sensitivity factor for an atom A is defined by

$$S_A = D(E_A)\cdot L_A \cdot T(E_A)\cdot Y_A \cdot G(J_A)\cdot A_A \cdot \sigma A(h\nu)\cdot \lambda_M(E_A)\cdot \sin\theta \tag{3}$$

It is generally agreed upon that a set of empirically derived sensitivity factors are adequate for quantification by means of XPS.[23,24] In our study we used the set of experimental atomic sensitivity factors provided by Kratos and expressed relative to the F 1*s* signal.

The calculation of the adsorbed amount of polyelectrolyte using XPS is facilitated by the fact that the mica crystal composition and in particular the chemical composition of the basal plane are well-known. The amount of polyelectrolyte adsorbed on mica was computed from the intensities of the N 1*s* and K 2*p* (or K 2s) photoelectron signals according to the method developed by Claesson et al.[25] and Herder et al.[26] In this method the number of exchangeable potassium (90−95%) and sodium (5−10%) ions located on the mica basal plane is used as an internal standard. This number corresponds to the negative aluminosilicate lattice charge on mica which amounts to 2.1 × 10^{14} per cm^2 according to Güven[27] and Gaines.[28]

The potassium and sodium ions on the mica surface are completely exchanged for protons upon immersion of the surfaces into aqueous solutions.[26,29] Ions situated in the mica crystal are not exchanged as mica does not swell in water. By measuring the potassium and sodium intensities before and after immersion, the change in intensity ΔI, of the K and Na signals can be related to the number of exchangeable ions on the surface. It can be shown that the signal intensity from the potassium ions located on the surface corresponds to a fraction f defined by eq 4 (after Herder)[26]

$$f = \frac{\Delta I_K}{I_K} \tag{4}$$

where I_K is the potassium signal from the bulk of the mica crystal and ΔI_K is the change in potassium intensity (or intensity

reduction upon exchange of potassium ions on the basal plane) which corresponds to the signal from the potassium ions initially lying on the mica surface. This fraction can be either measured or estimated theoretically from the layered structure of the mica crystal. In our case this value was determined experimentally.

The measured K 2*p* (or K 2*s*) signals in our experiments correspond to potassium ions from the bulk of the crystal. However, to account for the instrumental functions and to make the quantification absolute (given the fact that the total number of exchangeable potassium and sodium is known), it is convenient to relate the calculations to the number of exchanged potassium ions. Integration of eq 2 assuming a single atomic layer on the surface (in which case the photoelectrons come directly to the analyzer with no attenuation), yields eq 5:

$$\frac{\Delta N_{\mathrm{K}}}{A} = \frac{\Delta I_{\mathrm{K}}}{D(E_{\mathrm{K}}) \cdot L_{\mathrm{K}} \cdot T(E_{\mathrm{K}}) \cdot Y_{\mathrm{K}} \cdot G(J_{\mathrm{K}}) \cdot A_{\mathrm{K}} \cdot \sigma_{\mathrm{K}}(h\nu)} \quad (5)$$

where $\Delta N_{\mathrm{K}}/A$ is the surface density of exchangeable potassium ions. On the other hand, the surface density of potassium and sodium ions is related to the number of total exchangeable ions:

$$\frac{\Delta N_{\mathrm{K}}}{A} + \frac{\Delta N_{\mathrm{Na}}}{A} = 2.1 \cdot 10^{14}\ \frac{\text{ions}}{\text{cm}^2} \quad (6)$$

where ΔN is the respective number of exchanged ions and A is the area.

Equations 5 and 6 can be related if one accounts for the sodium content in the form of a constant $(1 + R)$:

$$\frac{\Delta N_{\mathrm{K}}}{A} + \frac{\Delta N_{\mathrm{Na}}}{A} = 2.1 \cdot 10^{14} = \frac{(1+R) \cdot \Delta I_{\mathrm{K}}}{D(E_{\mathrm{K}}) \cdot \mathrm{L}_{\mathrm{K}} \cdot T(E_{\mathrm{K}}) \cdot Y_{\mathrm{K}} \cdot G(J_{\mathrm{K}}) \cdot A_{\mathrm{K}} \cdot \sigma_{\mathrm{K}}(h\nu)} \quad (7)$$

and in terms of the measured potassium signal (that of the bulk potassium ions after immersing the mica in the respective solutions) one simply obtains

$$\frac{\Delta N_{\mathrm{K}}}{A} + \frac{\Delta N_{\mathrm{Na}}}{A} = 2.1 \cdot 10^{14} = \frac{(1+R) \cdot f \cdot I_{\mathrm{K}}}{D(E_{\mathrm{K}}) \cdot L_{\mathrm{K}} \cdot T(E_{\mathrm{K}}) \cdot Y_{\mathrm{K}} \cdot G(J_{\mathrm{K}}) \cdot A_{\mathrm{K}} \cdot \sigma_{\mathrm{K}}(h\nu)} \quad (8)$$

The experimentally obtained value for $(1 + R)f$ is 0.21 as accounted by Herder et al.[30] (n.b., in this reference the factor is called *FR*).

When polyelectrolyte is adsorbed, eq 8 must be modified so as to take into account the attenuation of the potassium signal due to the organic layer on the mica basal plane. The reduction of the potassium signal follows an exponential decay with the thickness of the layer given by eq 9:[23]

$$\bar{I}_{\mathrm{K}} = I_{\mathrm{K}} \cdot \exp\left(-\frac{d}{\lambda_{\mathrm{L}}{}^{\mathrm{K}} \cdot \sin\theta}\right) \quad (9)$$

where $\bar{I}_{\mathrm{K}}$ is the potassium signal when a layer (denoted by L) of thickness d is present.

If the polyelectrolyte is assumed to be adsorbed on the mica basal plane as a uniform layer of thickness d, and the nitrogen atoms are uniformly distributed across the layer (n_{A} independent of the distance x), integration of eq 2 with x between 0 and d, gives eq 10:

$$\frac{N_{\mathrm{N}}}{A} = \frac{I_{\mathrm{N}}\left(\frac{d}{\lambda_L^N(E_{\mathrm{N}}) \cdot \sin\theta}\right)}{D(E_{\mathrm{N}}) \cdot L_{\mathrm{N}} \cdot T(E_{\mathrm{N}}) \cdot Y_{\mathrm{N}} \cdot G(J_{\mathrm{N}}) \cdot A_{\mathrm{N}} \cdot \sigma_N(h\nu) \cdot \left[1 - \exp\left(\frac{d}{\lambda_{\mathrm{L}}{}^{\mathrm{N}}(E_{\mathrm{N}}) \cdot \sin\theta}\right)\right]} \quad (10)$$

Combining eqs 8, 9, and 10 and using experimental sensitivity factors as defined by eq 3, one can obtain the nitrogen density per unit area:

$$\frac{N_{\mathrm{N}}}{A} = \frac{I_{\mathrm{N}} \cdot S_{\mathrm{K}} \cdot \left(\frac{d}{\lambda_{\mathrm{L}}{}^{\mathrm{N}} \cdot \sin\theta}\right) \cdot \exp\left(-\frac{d}{\lambda_{\mathrm{L}}{}^{\mathrm{K}} \cdot \sin\theta}\right) \cdot 2.1 \cdot 10^{14}}{\bar{I}_{\mathrm{K}} \cdot S_{\mathrm{N}} \cdot (1+R)f \cdot \left[1 - \exp\left(-\frac{d}{\lambda_{\mathrm{L}}{}^{\mathrm{N}} \cdot \sin\theta}\right)\right]} \left(\frac{\lambda_{\mathrm{L}}{}^{\mathrm{N}}}{\lambda_{\mathrm{M}}{}^{\mathrm{K}}}\right) \quad (11)$$

Equation 11 can be rewritten in terms of known factors using the semiempirical relation $\lambda \propto E^{0.7}$ proposed by Wagner et al.,[31] where the kinetic energy (E) of emitted photoelectrons is given by the difference of the irradiated X-ray energy (1486.6 eV) and the binding energy for each element (see eq 12). In eq 12 we have also used the approximation that the decay constant in the standard matrix (λ_{M}) is equal to that in the layer (λ_{L}):

$$\frac{N_{\mathrm{N}}}{A} = \frac{I_{\mathrm{N}} \cdot S_{\mathrm{K}} \cdot \left(\frac{d}{\lambda^{\mathrm{K}} \cdot \sin\theta}\right) \cdot \exp\left(-\frac{d}{\lambda^{\mathrm{K}} \cdot \sin\theta}\right) \cdot 2.1 \cdot 10^{14}}{\bar{I}_{\mathrm{K}} \cdot S_{\mathrm{N}} \cdot (1+R)f \cdot \left[1 - \exp\left(-\frac{d}{\lambda^{\mathrm{K}} \cdot \sin\theta} \cdot \left(\frac{E_{\mathrm{N}}}{E_{\mathrm{K}}}\right)^{-0.7}\right)\right]} \quad (12)$$

where the reduced thickness, $d/\lambda^{\mathrm{K}} \cdot \sin\theta$, for the potassium signal is calculated from eq 9, i.e.:

$$\left(\frac{d}{\lambda^{\mathrm{K}} \cdot \sin\theta}\right) = \ln\left(\frac{I_{\mathrm{K}}}{\bar{I}_{\mathrm{K}}}\right) \quad (13)$$

Polymer Degradation in XPS Experiments. Due to the nature of the studied films (i.e., organic layers of polymers and cellulose), one may expect some damage during XPS analysis. This effect is not that important for the monochromatic source case where relatively little sample heating is involved. For an unmonochromatic source, however, the sample is much closer to the X-ray anode, and thermal degradation effects may be more important.[32]

There are three possible causes for polymer degradation under prolonged X-ray exposure in an XPS spectrometer: (a) interaction of X-ray photons with the polymer, (b) secondary electrons generated at the X-ray source and impinging the polymer surface, and (c) secondary electrons generated within the polymer. [2] It has been found, however, that the damage is mainly caused by X-rays rather than by electron bombardment.

Some investigators have found that poly(tetrafluorethylene) (or Teflon) suffered damage when exposed to monochromatic[33] and nonmonochromatic[34] X-rays in an XPS spectrometer. This damage was essentially observed as a depletion of fluorine in the near-surface region after long exposure times (typically 5−24 h). This has also been observed in the case of fluorocarbon surfactants.[35]

In general, however, it is claimed that other polymers are fairly stable under X-ray irradiation.[34,36−38] For example, non-

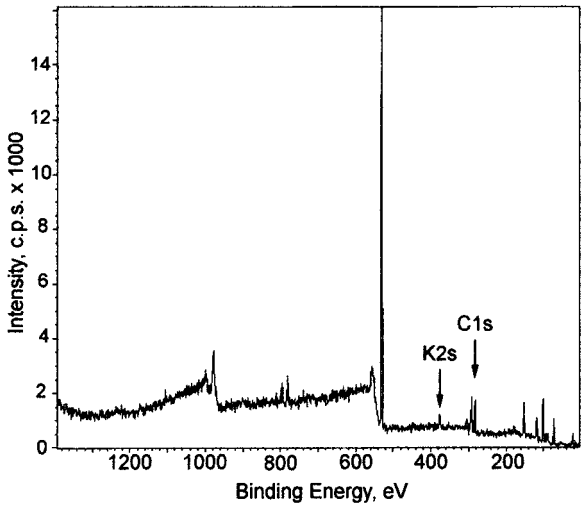

Figure 5. XPS survey spectrum of mica (after immersion in water) showing the major photoelectron and Auger electron lines (Al-*mono* mode).

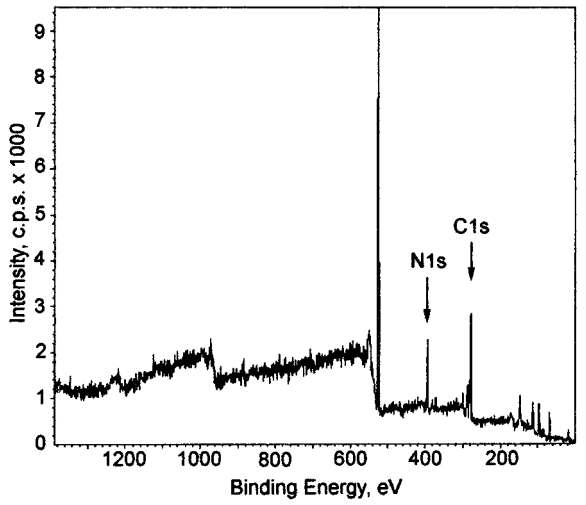

Figure 6. XPS survey spectrum after adsorption of AM-MAPTAC-1 on mica showing the major photoelectron and Auger electron lines (Al-*mono* mode).

fluorine-containing polymers were found to undergo considerable less beam damage at prolonged exposure times:[33] poly(methymethacrylate) (PMMA), polyacrylonitrile (PAN), poly(vinyl chloride) (PVC), and poly(ethyleneterephthalate) (PET) showed a much lower rate of elemental compositional change with X-ray exposure (changes 10 to 100 times lower than those observed in the case of fluorinated polymers).[33]

Experiments with poly(methyl methacrylate) showed that despite a reduction in the molecular weight (as inferred from solubility tests), X-ray irradiation of ca. 7 h produced no detectable changes in the XPS results.[38] Nitrogen-containing polymers (e.g., solid glycine) have been reported to suffer some radiation damage during exposure to X-rays,[39] but the reported damage did not affect the N 1*s* core level total intensity.

Ahmed et al.[40] reported on the damage of cellulosic materials after prolonged exposure to X-rays and heat in an XPS spectrometer. Fowler et al.[41] found that Ti X-rays produced reduction of cellulose nitrate after extended exposition, but Mg X-rays did not induce significant changes on the same surface after normal XPS exposure. Similarly, Ostmeyer et al.,[42] found that the surface of wood is not altered significantly during XPS analysis with Al X-rays.

From the foregoing examples it is obvious that certain polymers (specially fluor-containing polymers, or in general, halogen-containing polymers and surfactants) would suffer chemical changes under extended X-ray exposure. However, the damage in an XPS spectrometer can be kept to a minimum if the exposure time is not too long and proper cooling is ensured. In fact, experiments with layers of copolymers of AM-MAPTAC on mica and cellulose and with cellulose itself, did not reveal damage upon X-ray exposure during usual measurement times.

Results and Discussion

XPS Spectra and Operational Modes. Figure 5 shows a wide range or survey XPS spectrum for the mica surface (after immersion in water) using Al-*mono* operation. For comparison, a typical spectrum after adsorption of AM-MAPTAC-1 on mica is shown in Figure 6.

Comparison of these two spectra reveals that adsorption of the polyelectrolyte produces a distinctive N (N 1*s*) peak (from the nitrogen atoms in the copolymer) and a relative increase of the C (C 1*s*) signal due to the incorporation of the organic layer on the mica surface. Detailed spectra for N 1*s* and K 2*p* are shown in Figures 7 and Figure 8, respectively.

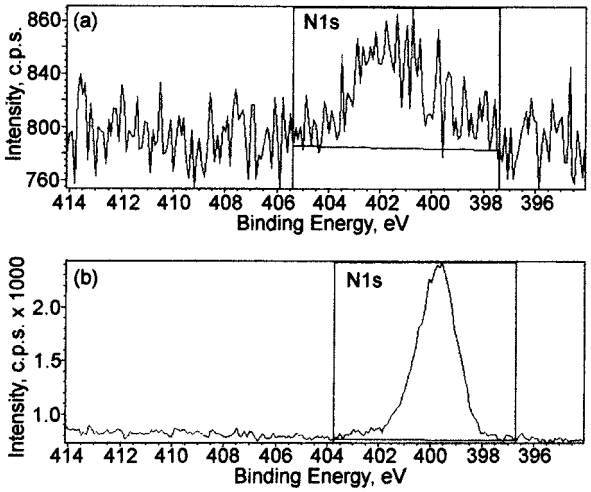

Figure 7. N 1*s* spectra for mica (a) and for polyelectrolyte (AM-MAPTAC-10) adsorbed on mica surface (b) (Al-*mono* mode).

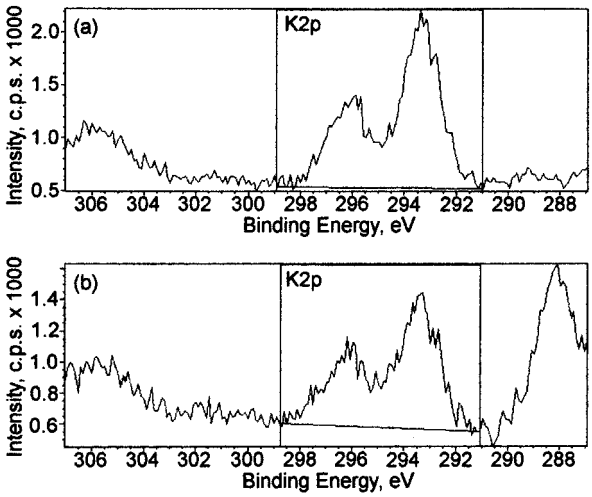

Figure 8. K 2*p* spectra for mica (a) and for polyelectrolyte (AM-MAPTAC-10) adsorbed on mica surface (b) (Al-*mono* mode).

It is clearly seen that upon adsorption of the polyelectrolyte on the mica basal plane the appearance of the N 1*s* peak is

TABLE 2: *f* and (*1 + R*) Factor for Different Operational Modes

operational mode	*f*	(1 + *R*)	*f*(1 + *R*)
Al-*elstat*, based on K 2*p* signal and 90°	0.18	1.095	0.197
Al-*elstat*, based on K 2*p* signal and 45°	0.172	1.146	0.197
Al-*mono*, based on K 2*p* signal and 90°	0.18	1.06	0.191
Al-*elstat*, based on K 2*s* signal and 90°	0.133	1.09	0.145

accompanied by an attenuation of the potassium signal at the same time as the C 1*s* peak increases. The intensities (raw areas) from these spectra are the key variables in the calculation of the adsorbed amount as explained in previous sections. It is important to note that for both operational modes (Al-*mono* and Al-*elstat*) related determinations can be based either on the K 2*s* or K 2*p* signals.

The factors *f* and *(1 + R)* can be determined using the XPS raw area for the potassium (K 2*p* or K 2*s*) and sodium (Na 1*s*) signals from bare and ion-exchanged mica (eqs 4 and 7). In these equations the K signal is first normalized using the Si 2*p* signal to get relative values which are not dependent on small differences in experimental setups between measurements.

The ion-exchanged mica is obtained after immersion of a freshly cleaved mica in pure water (see a representative spectrum in Figure 5). The ion-exchange process can be facilitated by addition of some acid to the aqueous media.

The factor *(1 + R)f* is not affected by the employed operational mode but only depends on the kinetic energy of the photoelectrons. This is demonstrated in Table 2 which includes a summary of the calculated values of *f* and *(1 + R)* for both operational modes. For the Al-*elstat* mode we determined these factors at two different angles between the sample surface and the emitted photoelectrons (45° and 90°).

In Table 2 the Al-*mono* K 2*s* value was not included because in this case the intensity is much lower than for the K 2*p* case, giving rise to some uncertainty. It is seen that for calculations based on K 2*p* signals the value of *f(1 + R)* is ca. 0.19, regardless of the operational mode. For calculations based on the K 2*s* signal the value is lower (0.145) as expected from the lower kinetic energy of the K 2*s* photoelectrons compared to that of the K 2*p* (1107 and 1192 eV, respectively). The relative amount of exchangeable potassium and sodium ions is easily calculated (from, e.g., Al-*elstat* K 2*p* data in first row of Table 2) to be 91 and 9%, respectively, in agreement with reported experimental values.[26]

Although the specific results on polyelectrolyte adsorption have not been presented yet (to be discussed in the next sections), it is convenient at this point to compare the results obtained after employing the XPS operational modes under investigation. As such, Figure 9 shows the calculated adsorbed amount of different polyelectrolytes on mica using either Al-*mono* or Al-*elstat* mode (both K 2*s* and K 2*p* signals).

Figure 9a clearly shows the excellent agreement between the calculated values for Al-*elstat* operational mode based on K 2*s* and K 2*p* signals. Considering inherent differences in the spectrometric measurements Figure 9c,d for different set of conditions (operational mode, samples, etc.), shows a very good agreement between Al-*mono* and Al-*elstat* modes (e.g., the average absolute deviation of the calculated adsorbed amount from Al-*mono* (K 2*p*) and Al-*elstat* (K 2*s*) is less than ca. 7%).

Although the use of an incident beam monochromator (Al-*mono*) is recommended for XPS analysis of organic materials (because of a lower risk of thermal damage due to the inherently less radiation and heat reaching the sample), the results presented in Figure 9 suggest that the use of a nonmonochromatic X-ray source (as in the case of Al-*elstat* mode) does not produce damage to the studied samples (or more correctly, does not produce (if any) further damage as compared to that caused by operating in Al-*mono* mode).

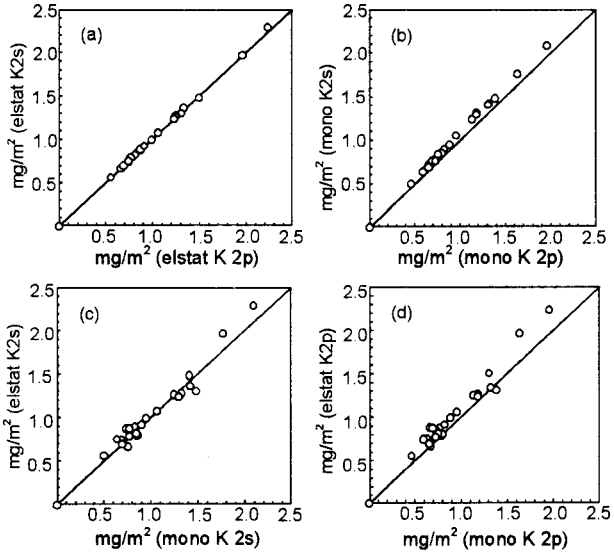

Figure 9. Adsorbed amount of polyelectrolyte on mica according to different XPS modes.

In Al-*mono* mode the calculated adsorbed amount based on K 2*s* signals is a little higher compared to that based on K 2*p* signals (see Figure 9b).

From the discussion presented above and from the fact that in the Al-*elstat* mode the signal intensity is much higher and therefore weak peaks are measured more accurately (at least for samples with very low adsorbed amount of polyelectrolyte), it was considered convenient to use the results from Al-*elstat* operational mode in the discussion on polyelectrolyte adsorption presented in the sections that follow (for AM-MAPTAC-1; however, the Al-*mono* values are used since for this case more data were collected under this mode).

Silicon Signal Check. The ratio of potassium to silicon atoms as calculated from the measured intensity signals for all the experiments can be used as a check for the consistency of XPS measurements. This ratio (see eq 14) was calculated after integration of eq 2, using integration limits between 0 and ∞ (the case of a homogeneous bulk material), and considering the exponential attenuation of the signal intensity for each element due to the adsorbed polyelectrolyte overlayer:

$$\frac{\left(\frac{N_K}{A}\right)}{\left(\frac{N_{Si}}{A}\right)} = \frac{\bar{I}_K}{\bar{I}_{Si}} \frac{S_{Si}}{S_K} \exp\left(\left(\frac{d}{\lambda_L{}^K \sin\theta}\right) - \left(\frac{d}{\lambda_L^{Si} \sin\theta}\right)\right) \quad (14)$$

The ratio obtained for different sets of experiments was between 0.24 and 0.25. Considering the sensitivity of the signal to the various factors involved, the narrow margin for this ratio indicates good consistency in the measurements. The measured ratio is, however, different from that calculated for the theoretical elemental composition of the mica bulk crystal, i.e., 0.33 (assuming $KAl_2(AlSi_3O_{10})(OH)_2$ as elemental formula). This difference is simply explained by three factors that contribute to the observed reduction, i.e., no contribution to the signal from the outermost layer of potassium ions that were exchanged, differences in the inelastic mean free paths, and electron diffraction.[43,44]

Nitrogen Detection in the Adsorbed Layer. The XPS nitrogen signal is distinctive of adsorbed polyelectrolytes on

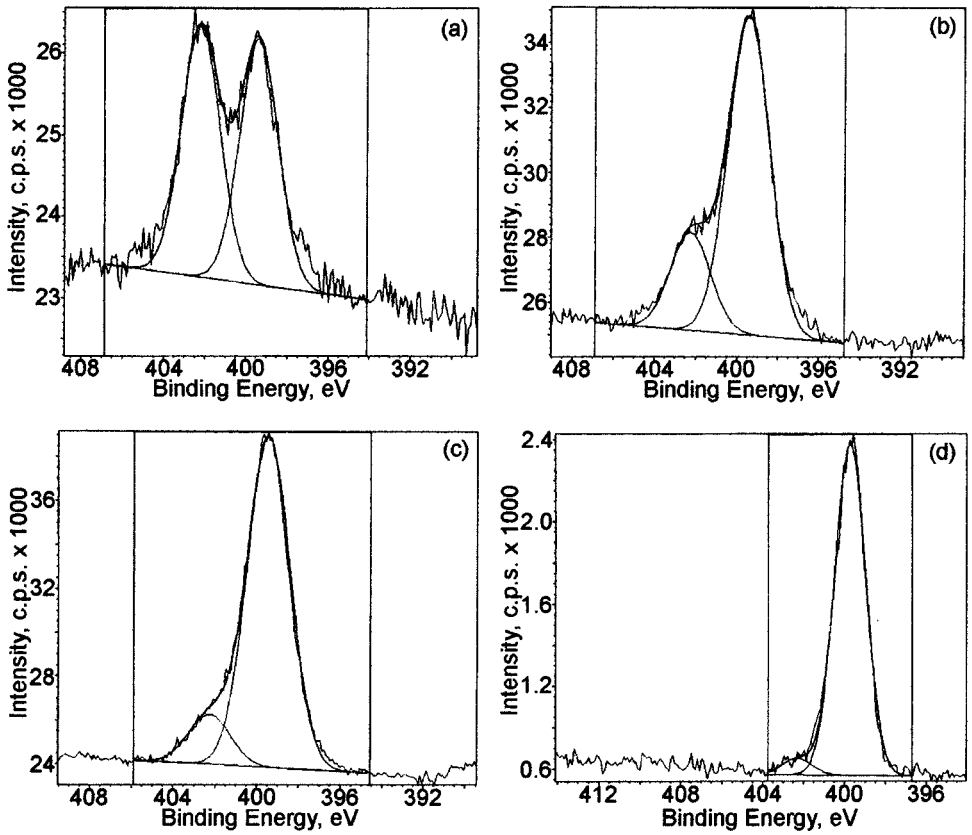

Figure 10. Nitrogen 1*s* spectra for polyelectrolytes of different charge densities adsorbed on mica: AM-MAPTAC-100 (100% charge density) (a); AM-MAPTAC-30 (30% charge density) (b); AM-MAPTAC-10 (10% charge density) (c); and AM-MAPTAC-1 (1% charge density) (d). Note: Al-*elstat* mode for (a)−(c) and Al-*mono* for (d).

mica since this substrate does not bare any nitrogen atom. The polyelectrolytes studied, on the other hand, carry nitrogen atoms in two different functional groups, i.e., in amide bonds and ammonium groups. Specifically, AM monomeric units carry one (amide) nitrogen per unit and MAPTAC monomeric units carry two nitrogens per unit (one forming the amide bond and the other in the charged ammonium group).

The N 1*s* signal in the form of amide groups appears as a peak at a binding energy of about 400 eV [24] (399.8 eV for PAM, when C 1*s* is at 285.0 eV, according to Beamson and Briggs).[32] In an ammonium salt the peak is shifted toward higher binding energy (ca. 401−403 eV).[24] For example, for $-N(CH_3)_3^+$ in poly(vinylbenzyltrimethylammonium chloride (or PVBTMAC)) the peak is shifted to 402.1 eV,[32] i.e., there is a shift of ca. 2−3 eV.

Therefore, since in AM-MAPTAC-100 there is equal number of nitrogen from amide bond and ammonium nitrogen, two peaks of similar intensities and separated by about 2−3 eV are expected (for example in the case of PAM and PVBTMAC the peak separation is 2.3 eV). In fact, after performing curve fitting, it was found that in our case (MAPTAC) the peaks are separated by ca. 2.6−2.9 eV (see Figure 10).

Figure 10 includes detailed spectra for polyelectrolytes of different charge density. Figure 10a shows the case of poly(MAPTAC) ($\tau = 100\%$) and Figure 10b−d shows the respective spectra for decreasing polyelectrolyte charge densities (from 30 to 1%, respectively).

Deconvolution of the nitrogen peaks (as those shown in Figure 10) allows the estimation of the relative distribution of nitrogen-containing groups in the adsorbed layer as illustrated in Table 3. The calculated percents of ammonium N from XPS spectra using Al-*mono* mode are 51.3, 24.2, and 12.7 for AM-MAPTAC-100, -30, and -10, respectively. For both modes of operation (Al-*mono* or Al-*eslstat*), the proportion of nitrogen from ammonium quarternarium groups (i.e., proportion of charged nitrogens relative to the total number of nitrogens), indicates good agreement between XPS measurements and expected values (calculated from the charge density and corresponding polyelectrolyte structure) (see Table 3). For AM-MAPTAC-1, curve fitting to determine the % of quarternarium ammonium N is more difficult since these groups are present in a much lower proportion.

TABLE 3: Molar Percentage of Quarternarium Ammonium Nitrogen after Deconvolution of N 1*s* (Al-*elstat*) Spectra from XPS Measurements of Polyelectrolyte Adsorbed on Mica[a]

adsorbed polyelectrolyte	polyelectrolyte charge density (τ)	% ammonium N from XPS spectra	% ammonium N calcd from structure
AM-MAPTAC-100	100	50.6	50.0
AM-MAPTAC-30	30	22.9	23.1
AM-MAPTAC-10	10	12.7	9.1
AM-MAPTAC-1	1	3−4	0.95

[a] For comparison, the expected values calculated from the polyelectrolyte charge density and structure are also included.

The results for the 10% and 1% charge polyelectrolytes indicate a higher charge density of the adsorbed polymer compared to that calculated from the structure. It can be argued that there may be a slight preferential adsorption of the fraction of these polyelectrolytes with charge density higher than the average one (one has to remember that there is polydispersity in both molecular weight and charge density).

Adsorption of Low-Charge-Density Polyelectrolytes on Cellulose. The adsorption of copolymers of AM-MAPTAC on regenerated cellulose was estimated from XPS analysis of

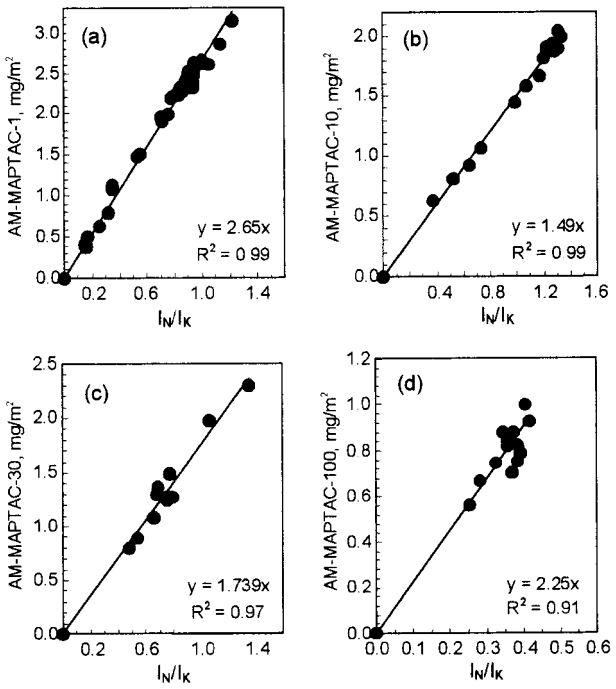

Figure 11. Linear relationship between the polyelectrolyte adsorbed amount and the ratio of the signal intensity for nitrogen to potassium atoms for AM-MAPTAC-1 (a), AM-MAPTAC-10 (b), AM-MAPTAC-30 (c), and AM-MAPTAC-100 (d).

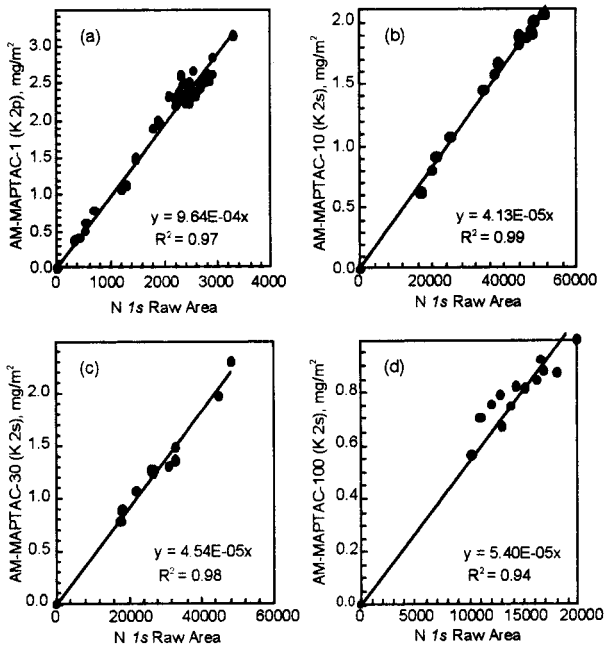

Figure 12. Calibration curves for the estimation of the amount of adsorbed polyelectrolyte on cellulose in the case of AM-MAPTAC-1 (a), AM-MAPTAC-10 (b), AM-MAPTAC-30 (c), and AM-MAPTAC-100 (d).

samples after adsorption for 18−24 h. The number of TMSC layers on mica used in each experiment (80 layers) as a precursor of the cellulose film was selected so as to produce a thick enough coating to nullify contributions to the photoelectron signals from nitrogen atoms contained in the AA/EA layer used to hydrophobize the mica prior to TMSC deposition. The complete regeneration of cellulose after desilylation of the TMSC films was confirmed by the absence of silicon peaks in the XPS spectra of the respective surfaces.

For small variations of the adsorbed polyelectrolyte layer thickness, Taylor expansion of eq 12 reveals that the surface density of nitrogen atoms is proportional to the ratio of the signal intensity for nitrogen to potassium atoms ($I_N/\bar{I}_K$). It is thus possible to construct "calibration" curves of nitrogen number density (or polyelectrolyte adsorbed amount) vs $I_N/\bar{I}_K$ (as obtained from raw areas in XPS spectra for each of the used polyelectrolytes). By using such calibration curves it is thus possible to easily and accurately quantify the adsorbed amount.

A set of calibration curves obtained from the previously presented XPS data for the adsorption of polyelectrolytes on mica is shown in Figure 11. As can be seen from the regression coefficient values (inserts of Figure 11), there is excellent agreement between the experimental data points and the proposed calibration curve, specially for high adsorbed amounts (e.g., AM-MAPTAC-1 and -10 cases). For small adsorbed amounts (e.g., the AM-MAPTAC-100 case) the estimation of the adsorbed amount is less accurate due to the fact that the nitrogen signal is smaller and the relative errors become more important.

It is obvious that the approach aboved mentioned would prove most useful in the quantitative determination of polymer-adsorbed amount on other substrates different than mica. As such, we applied this methodology to cellulose substrates. Since the cellulose layer thickness is very large, the potassium signal is absent and therefore it is not possible to evaluate the ratio $I_N/\bar{I}_K$. Nevertheless, if regression curves are obtained using the adsorbed polyelectrolyte amount and the nitrogen signal intensity, it turns out that a linear relationship is also observed (see in Figure 12 the corresponding curves for the polyelectrolytes). This calibration curve is most accurate for small adsorbed amounts, i.e., when the variation of $\bar{I}_K$ is small. In the case of Al-*elstat* K 2*p* and Al-*mono* K 2*p* operational modes, linear calibration curves as those shown in Figure 12, were also obtained (data not shown).

The adsorption of low-charge-density AM-MAPTAC copolymer ($\tau = 1\%$) on cellulose was explored for polyelectrolyte concentrations between 10 and 500 μg/mL. Figure 13 illustrates typical XPS wide spectrum and N 1*s* detailed spectrum for cellulose surfaces after immersion in a 0.1 mM KBr aqueous solution (Figure 13) and following, in an immersion in the same solution containing 500 μg/mL of AM-MAPTAC-1 (Figure 14). The magnitude of the N 1*s* peak in the latter case demonstrates with no doubt that nitrogen-containing polyelectrolyte was adsorbed on the cellulose surface. The same observation applies to the rest of the experiments involving polyelectrolytes with different charge densities at various concentrations.

Figure 15 shows the adsorption isotherm on cellulose. For comparison purposes the adsorption isotherm for the same polyelectrolyte (AM-MAPTAC-1) on bare mica is included in this figure. It is apparent that the adsorption is considerably higher on the highly negatively charged mica surface as compared to the (nearly) uncharged cellulose surfaces.[20,45,46]

Similar experiments were performed with AM-MAPTAC polyelectrolytes of different charge densities. From the plateau adsorbed amount measured for polyelectrolytes of 1, 10, 30, and 100% charge density, Figure 16, it is demonstrated that the adsorbed amount decreases with the linear charge density of the polyelectrolyte.

Figure 17 illustrates the effect of the polymer charge density on the number density of charged segments adsorbed on the cellulose surface. It can be seen that the charge segment density is largest for the 100% charged polyelectrolyte. From the fact that the different polyelectrolytes do not adsorb with the same

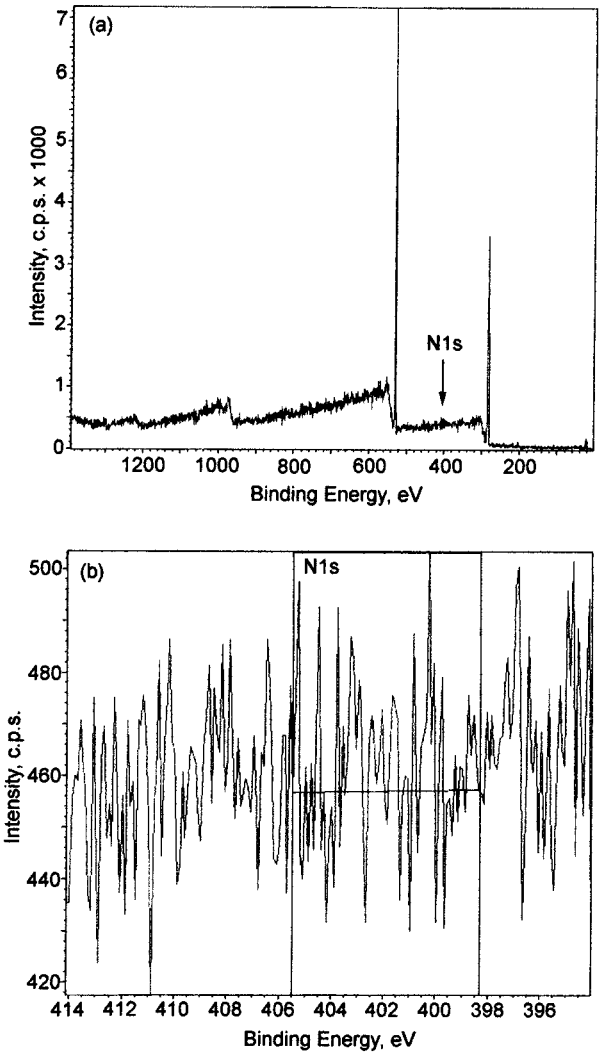

Figure 13. XPS wide spectrum (a) and detailed N 1*s* spectrum (b) for cellulose after immersion in 0.1 mM KBr solution.

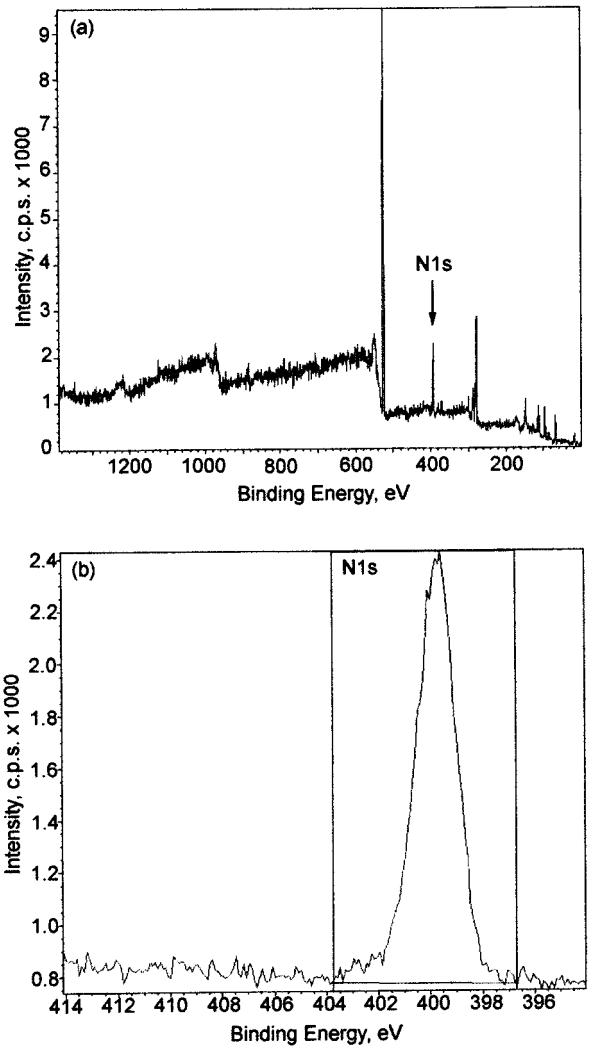

Figure 14. XPS wide spectrum (a) and detailed N 1*s* spectrum (b) for cellulose after immersion in 0.1 mM KBr solution containing 500 mg/mL of AM-MAPTAC-1.

number of charged segments it is not generally correct to use the adsorbed amount of polyelectrolytes to determine the surface charge density on cellulose, even though this method may work under special circumstances.[47] The observed behavior is due to the fact that nonelectrostatic factors are also of importance for the adsorption on cellulose substrates (which is a low charge density surface).

It is interesting to note that although the polyelectrolyte adsorbed amount on cellulose is smaller than in the case of mica surfaces, the adsorption behavior in terms of the effect of the polyelectrolyte charge density is similar for both surfaces, i.e., a plateau adsorption maximum at low polyelectrolyte charge density. Despite the fact that the adsorption of polyelectrolyte on cellulose is thought to be mainly driven by nonelectrostatic interactions**,** it seems that an electrostatic component is also involved in the adsorption phenomena. It has been argued from surface force experiments that similar LB-cellulose films (at pH 5.6) are not charged.[20] However, recent results indicate that the cellulose layer swells at pH 7,[48,49] which may be an indication of an increased number of charges. Washed cellulosic fibers and fines, on the other hand, always take on a negative charge due to the ionization of surface groups, mainly oxidized hemicelluloses, cellulose, and lignin.[50−52] In the case of the present LB-cellulose, the only likely source of negative charge is carboxyl groups since the pK_a of other possible sources, e.g.,

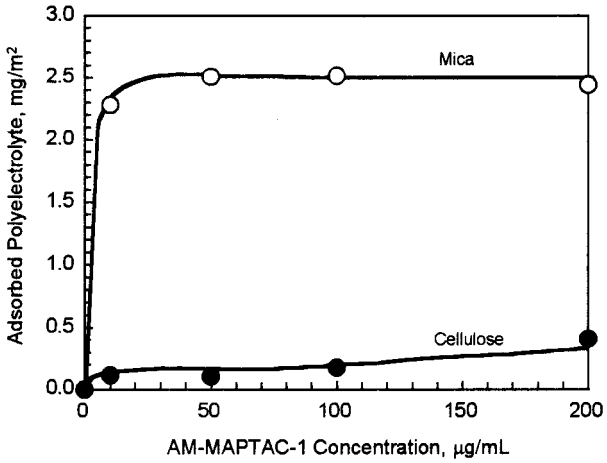

Figure 15. Adsorption isotherm for AM-MAPTAC-1 on bare mica and cellulose in 0.1 mM KBr aqueous solution.

sugar alcoholic groups and hemiacetal OH groups is above 12.[53] Findings on other model cellulose surfaces, e.g., spin-coated cellulose (prepared from microcrystalline cellulose) studied by surface force techniques[54,55] and type II cellulose studied by scanning probe microscopy[56] support the thesis of a charged cellulose surface.

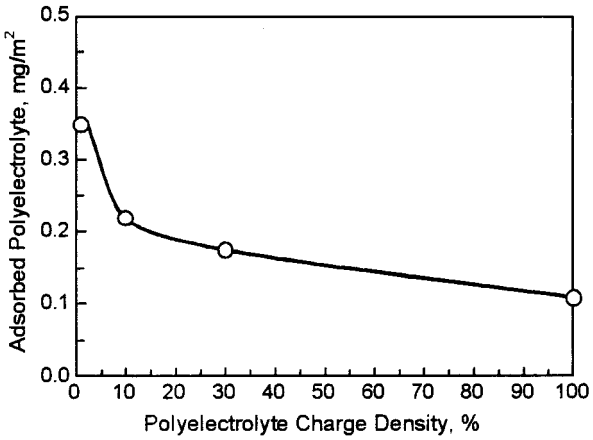

Figure 16. Plateau-adsorbed amount for copolymers of AM-MAPTAC of different charge densities on cellulose.

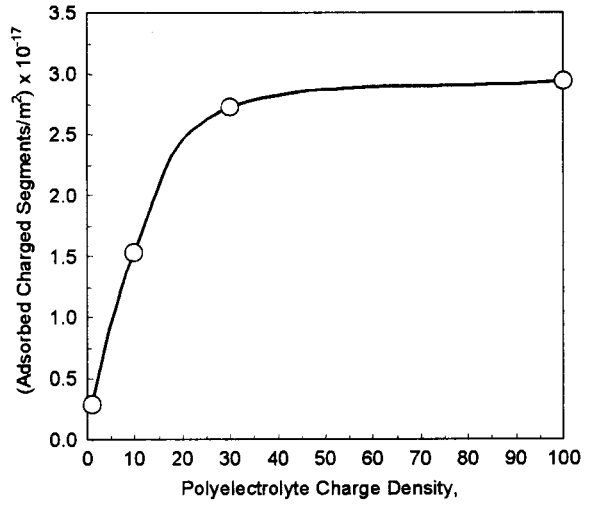

Figure 17. Charged segment number density of AM-MAPTAC copolymers adsorbed on cellulose.

Conclusions

A procedure based on XPS measurements to estimate the absolute amount of copolymers of acrylamide that adsorbs on mica surfaces in aqueous media has been successfully achieved. The calculation of the adsorbed amount takes advantage of the knowledge of the mica crystal composition at the basal plane and its ion-exchange properties in aqueous solution. Good agreement between the employed methodologies, i.e., operation of the spectrometer with monochromator (with characteristic low X-ray intensities) and with unmonochromatized Al X-rays (of higher intensities), not only revealed soundness in the calculation procedure but also that possible effects from sample damage are minimal.

The measurements of the amount of cationic polyelectrolyte adsorbed on cellulose in aqueous solutions was achieved using XPS calibration curves obtained from adsorption data for the same polyelectrolytes on bare mica surfaces.

An electrostatic driving force for the polyelectrolyte adsorption on cellulose is important below the charge neutralization point. However, a slight recharging of the cellulose surface is observed at high polyelectrolyte concentrations[20,46] which demonstrates that also nonelectrostatic interactions have to be considered. This is supported by the observation in the current study that shows that the number of charged segments is different for the different polyelectrolytes used.

Acknowledgment. Mikael Sundin is acknowledged for his contribution in XPS measurements. O.J.R. thankfully acknowledges support from the Scientific and Technologic Council (CDCHT) of Universidad de Los Andes. R.D.N. and O.J.R. also gratefully acknowledge the financial support provided by the NRI Competitive Grants Program/USDA under Grant No. 95-37103-2060. P.C. acknowledges financial support from the Competence Centre for Surfactants Based on Natural Products (SNAP) and the SSF program "Colloid and Interface Technology".

References and Notes

(1) Ratner, B. D.; Yoon, S. C.; Mateo, N. B. Surface Studies by ESCA of Polymers for Biomedical Applications. In *Polymer Surfaces and Interfaces*; Feast, W. J., Munro, H. S., Eds.; John Wiley and Sons: Chichester, 1987; p 231.

(2) Chan, C.-M. *Polymer Surface Modification and Characterization*; Carl Hanser Verlag: Kempten, 1994.

(3) Ström, G.; Carlsson, G.; Schulz, A. *Nordic Pulp Paper Res. J.* **1993**, *8*, 105−112.

(4) Hemminger, C. S. *ESCA Analysis as a Tool to Study Surfaces of Treated Paper*; TAPPI Coating Conference, 1985, Atlanta.

(5) Arai, T.; Yamasaki, T.; Suzuki, K.; Ogura, T.; Sakai, Y. *Tappi J.* **1988**, *71*, 47−52.

(6) Engstrom, G.; Strom, G.; Norrdahl, P. *Tappi J.* **1987**, *70*, 45−49.

(7) Fujiwara, H.; Kline, J. E. *ESCA of Pigment-Coated Paper*; International Process and Materials Quality Evaluation Conference, 1986, Atlanta.

(8) Brinen, J. S.; Calbick, J. C.; Cody, R. D. *Surface Interface Anal.* **1989**, *14*, 245−249.

(9) Dorris, G. M.; Gray, D. G. *Cellulose Chem. Technol.* **1978**, *12*, 9−23.

(10) Dorris, G. M.; Gray, D. G. *Cellulose Chem. Technol.* **1978**, *12*, 721−734.

(11) Gray, D. G. *Cellulose Chem. Technol.* **1978**, *12*, 735−743.

(12) Laine, J.; Stenius, P.; Carlsson, G.; Ström, G. *Cellulose* **1994**, *1*, 145−160.

(13) Laine, J.; Stenius, P.; Carlsson, G.; Ström, G. *Nordic Pulp Paper Res. J.* **1996**, *3*, 201−210.

(14) Mjöberg, P. J. *Cell. Chem. Technol.* **1981**, *15*, 481−486.

(15) Stenius, P.; Laine, J. *Appl. Surf. Sci.* **1994**, *75*, 213-219.

(16) Ödberg, L.; Ström, G. *Svensk Papperstid.* **1983**, *86*, R141−R145.

(17) Takeyama, S.; Gray, D. G. *Cell. Chem. Technol.* **1982**, *16*, 133−142.

(18) Stein, A. Ph.D. Dissertation, Friedrich-Schiller-Universität, 1991.

(19) Berg, J. M.; Eriksson, L. G. T.; Claesson, P. M.; Nordli Børve, K. G. *Langmuir* **1994**, *10*, 1225.

(20) Holmberg, M.; Berg, J.; Stemme, S.; Ödberg, L.; Rasmusson, J.; Claesson, P. *J. Colloid Interface Sci.* **1997**, *186*, 369−381.

(21) Schaub, M.; Wenz, G.; Wegner, G.; Stein, A.; Klemm, D. *Adv. Mater.* **1993**, *5*, 919.

(22) Seah, M. P. *Surf. Interface Anal.* **1980**, *2*, 222.

(23) Briggs, D.; Seah, M. P. *Practical Surface Analysis. Vol. 1: Auger and X-ray Photoelectron Spectroscopy*, 2nd. ed.; Wiley: Chichester, 1990.

(24) Wagner, C. D. *Anal. Chem.* **1977**, *49*, 1282.

(25) Claesson, P. M.; Blom, C. E.; Herder, P. C.; Ninham, B. W. J. *J. Colloid Interface Sci.* **1986**, *114*, 234−242.

(26) Herder, P. C.; Claesson, P. M.; Herder, C. E. *J. Colloid Interface Sci.* **1987**, *119*, 155.

(27) Güven, N. *Z. Kristallogr.* **1971**, *83*, 531.

(28) Gaines, G. L. *Nature* (London) **1956**, *178*, 1304.

(29) Claesson, P. M.; Herder, P. C.; Eriksson, J. C.; Stenius, P.; Pashley, R. M. *J. Colloid Interface Sci.* **1986**, *109*, 31.

(30) Herder, P. C. Surfactant adsorption on mica studied by surface force and ESCA measurement. Ph.D. Dissertation, Royal Institute of Technology, 1988.

(31) Wagner, C. D.; Davis, L. E.; Ribbs, W. M. *Surf. Interface Anal.* **1980**, *2*, 53.

(32) Beamson, G.; Briggs, D. *High-Resolution XPS of Organic Polymers. The Scienta ESCA300 Database*; Wiley: Chichester, 1992.

(33) Chaney, R.; Barth, G. An ESCA Study on the X-ray Induced Changes in Polymeric Materials. In *Polymer Surface Dynamics*; Andrade, J. D., Ed.; Plenum Press: New York, 1988; pp 171−178.

(34) Wheeler, D. R.; Pepper, S. V. *J. Vac. Sci. Technol.* **1982**, *20*, 226.

(35) Claesson, P. M.; Herder, P. C.; Berg, J. M.; Christenson, H. K. *J. Colloid Interface Sci.* **1990**, *136*, 541.

(36) Akhter, S.; Allan, K.; Buchanan, J. A.; Cook, A.; Campion, A.; White, J. M. *Appl. Surface Sci.* **1988−1989**, *35*, 241.

(37) Storp, S. *Spectrochim. Acta* **1985**, *40B*, 745.
(38) Buchwalter, L. P.; Czornyj, G. *J. Vac. Sci. Technol.* **1990**, *A8*, 781.
(39) Chan, D.; Healy, T. W.; White, L. R. *J. Chem. Soc., Faraday Trans. 1* **1976**, *72*, 2844−2865.
(40) Ahmed, A.; Adnot, A.; Grandmaison, J. L.; Kaliaguine, S.; Doucet, J. *Cellulose Chem. Technol.* **1987**, *21*, 483−492.
(41) Fowler, A. H. K.; Munro, H. S.; Clark, D. T. *Cellulose and Its Derivatives: Chemistry, Biochemistry and Applications*; John Wiley: New York, 1985.
(42) Ostmeyer, J. G.; Elder, T. J.; Littrell, D. M.; Tatarchuk, B. J.; Winandy, J. E. *J. Wood Chem. Technol.* **1988**, *8*, 413−439.
(43) Evans, S.; Raftery, E.; Thomas, J. M. *Surf. Sci.* **1979**, *89*, 64.
(44) Adams, J. M.; Evans, S.; Thomas, J. M. *J. Am. Chem. Soc.* **1978**, *100*, 3260.
(45) Holmberg, M.; Wigren, R.; Erlandsson, R.; Claesson, P. M. *Colloids Surf. A* **1997**, *129−130*, 175−183.
(46) Poptoshev, E.; Rutland, M. W.; Claesson, P. M. *Langmuir* **2000**, *16*, 1987−1992.
(47) Winter, L.; Wägberg, L.; Ödberg, L.; Lindström, T. *J. Colloid Interface Sci.* **1986**, *111*, 537.
(48) Carambassis, A.; Rutland, M. *Langmuir* **1999**, *15*, 5584.
(49) Österberg, M.; Claesson, P. M. *J. Adhes. Sci. Technol.* **2000**, *14*, 603−618.
(50) Au, C. O.; Thorn, I. *Applications of Wet-End Paper Chemistry*; Blackie Academic & Professional: Cambridge, U.K., 1995.
(51) Scott, W. E. *Principles of Wet End Chemistry*, 2nd ed.; Tappi Press: Atlanta, GA, 1996.
(52) Roberts, J. C. *Paper Chemistry*; Blackie-Chapman and Hall: New York, 1991.
(53) Eklund, D.; Lindström, T. *Paper Chemistry: An Introduction*; DT Paper Science: Grankulla, Finland, 1991.
(54) Neuman, R.; Rojas, O. *Interparticle Forces in Papermaking*; 5th Venezuelan Pulp and Paper Conference, 1996, Maracay (Venezuela).
(55) Neuman, R. D.; Berg, J. M.; Claesson, P. M. *Nordic Pulp Paper Res. J.* **1993**, *8*, 96.
(56) Rutland, M. W.; Carambassis, A.; Willing, G.; Neuman, R. D. *Colloids Surf., A: Physicochem. Eng. Aspects* **1997**, *123−124*, 369−374.